

www.acsami.org Research Article

Solution-Processable PEDOT Particles for Coatings of Untreated 3D-Printed Thermoplastics

Yang Lu, → Haoru Yang, → Yifan Diao, Hongmin Wang, Chiemela Izima, Imani Jones, Reagan Woon, Kenneth Chrulski, and Julio M. D'Arcy*



Cite This: ACS Appl. Mater. Interfaces 2023, 15, 3433-3441



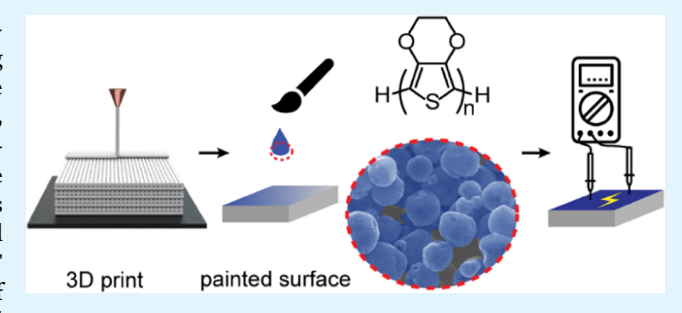
ACCESS

III Metrics & More

Article Recommendations

Supporting Information

ABSTRACT: Lack of solution processability is the main bottleneck in research progression and commercialization of conducting polymers. The current strategy of employing a water-soluble dopant (such as PEDOT:PSS) is not feasible with organic solvents, thus limiting compatibility on hydrophobic surfaces, such as three-dimensional (3D) printable thermoplastics. In this article, we utilize a colloidal dispersion of PEDOT particles to overcome this limitation and formulate an organic paint demonstrating conformal coating on 3D-printed objects. We start with synthesizing PEDOT particles that possess a low electrical resistance (gap resistance of 4.2 \pm 0.5 Ω/mm). A particle-based organic paint is formulated and



applied via brush painting. Coated objects show a surface resistance of 1 k Ω /cm, comparable to an object printed by commercial conductive filaments. The coating enables the fabrication of pH and strain sensors. Highly conductive PEDOT particles also absorb light strongly, especially in the near-infrared (NIR) range due to the high concentration of charge carriers on the polymer's conjugated backbones (i.e., polarons and bipolarons). PEDOT converts light to heat efficiently, resulting in a superior photothermal activity that is demonstrated by the flash ignition of a particle-impregnated cotton ball. Consequently, painted 3D prints are highly effective in converting NIR light to heat, and a 5 s exposure to a NIR laser (808 nm, 0.8 mW/cm²) leads to a record high-temperature increase (194.5 °C) among PEDOT-based coatings.

KEYWORDS: PEDOT particles, aerosol synthesis, organic processability, thermal plastic, organic paint, 3D printing, flash ignition, NIR photothermal

■ INTRODUCTION

Expanding the functionalities of three-dimensional (3D) printed objects beyond their basic structural functions gains importance as 3D printing becomes a popular method of manufacturing.¹ A common form of 3D printing, fused deposition modeling (FDM), is inexpensive and works with varying levels of resources, as it can be implemented at the household level.² FDM's accessibility means it has the capacity to make societal impacts across disciplines, especially with the production of 3D-printed objects with high electrical conductivity. The exploration of electronic and thermal capabilities in 3D-printed materials is of paramount importance for developing applications ranging from energy storage to biotechnologies. Notably, 3D printing is used to create custom, patient-specific medical constructs, such as hearing aids and prosthetics, and to fabricate electrochemical energy storage devices such as batteries and capacitors.^{3,4} However, 3D printing objects from commercially conductive filaments has limitations. Conductive filaments typically consist of carbon, which can be tough on the typically soft nozzles used in FDM printers.⁵ Aside from FDM, other methods for 3D printing electronics have their own limitations. For

example, the use of surface direct write techniques to print with conductive filaments can require expensive equipment, the printers can get clogged, and the 3D printing capacity of the technology that tries to circumvent those clogging issues is often limited.⁶ Freeform 3D printing techniques using conductive metal filaments and inks necessitate high-temperature sintering; or exist in a liquid form, which limits their practicality in applications.⁶ Conformally coating untreated 3D-printed thermoplastics with functional and robust film or paint is needed to impart electrical conductivity and provide a viable alternative to conductive commercial filaments.

Conducting polymers possess unique electronic, ionic, and optical properties with the potential for advancing the next generation of bioelectronics, energy harvesting/storage electrodes, and electrochemical catalysts. Unfortu-

Received: October 11, 2022 Accepted: December 16, 2022 Published: January 3, 2023





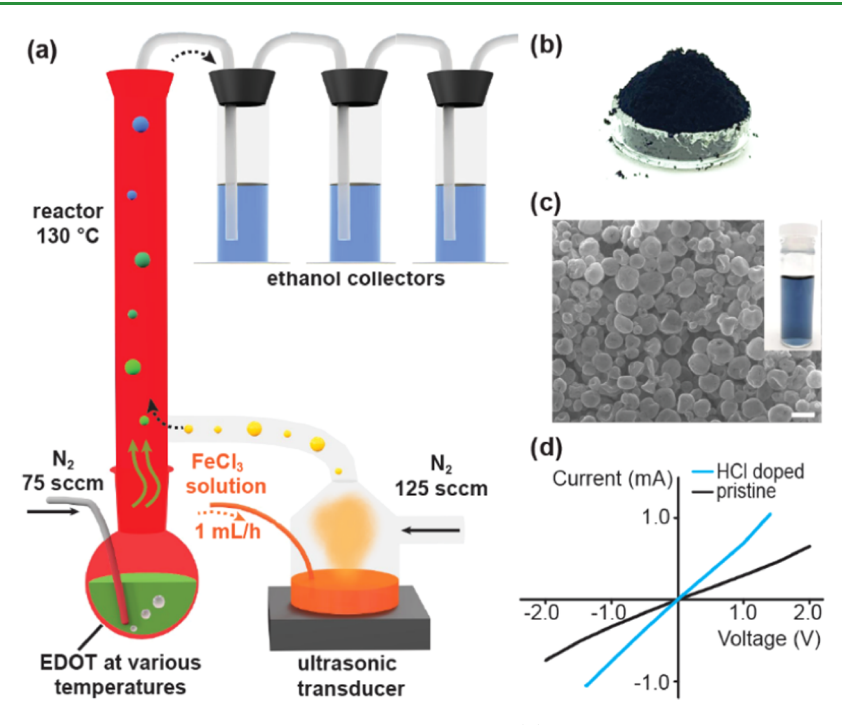


Figure 1. (a) Flow process diagram of aerosol vapor phase polymerization reactor. (b) Purified and lyophilized particles are collected as a powder. (c) Scanning electron micrograph of spherical and discrete PEDOT particles (scale bar is 1 μ m). The inset shows particles dispersed in water. (d) Current—voltage curves demonstrate ohmic behavior and a steeper slope (blue curve) for HCl-vapor-doped particles.

nately, the recalcitrant insolubility for the vast majority of conducting polymers remains a challenge stifling the development of current and future applications. Among conducting polymers, poly(3,4-ethylenedioxythiophene) polystyrene sulfonate (PEDOT:PSS) is a solution-processable exception commonly purchased as a water-based formulation 15 suitable for inkjet printing, ¹⁶ drop casting, and spin coating. ^{17,18} A major limitation for PEDOT:PSS stems from its incompatibility with organic solvents, leading to coatings that readily delaminate from untreated hydrophobic substrates such as 3Dprinted thermoplastics. An alternative to processing a solutionbased formulation is found by dispersing conducting polymer particles as colloids; 19 however, few reports in the literature discuss the synthesis and optimization of solution-processable conductive PEDOT particles. 20-22 Here, we develop a continuous aerosol synthesis that produces submicron PEDOT particles of low electrical resistance (4.2 \pm 0.5 Ω) processable in organic solvents, affording a stable dispersion (surfactant is unnecessary) for conformally coating untreated 3D-printed thermoplastics. A particle-based coating is robust, electrically conductive (1 k Ω /cm), and enables the engineering of stretchable resistive sensors. Moreover, our coatings are highly photothermally active because PEDOT's charge carriers absorb light in the near-infrared (NIR) region. Exposing a coating to a 5 s laser pulse (808 nm, 0.8 mW/cm²) raises its temperature to 194.5 °C, the highest reported among PEDOT coatings, 23,24 with the potential for light-induced surface sterilization applications.

■ MATERIALS AND METHODS

Iron(III) chloride (reagent grade, 97%), ethanol (200 proof, anhydrous), and 3,4-ethylenedioxythiophene (EDOT, 97%) were purchased from Sigma Aldrich and used without further purification. Ultrapure water was obtained from a Millipore filter (18.2 M Ω). 3D printing filaments were purchased from eSUN (PLA and PETG,

brand name: Inland) and Ninjiatek (TPU, brand name: NinjiaFlex). Conductive PLA filaments were purchased from Proto-Pasta.

Particle Synthesis and Purification. A straight Vigreux tube 60 cm in length and 2.54 cm in diameter was held vertically as the reactor and heated to 130 $^{\circ}$ C; the finger indentations inside the glass reactor disturbed the gas streams for better reactant mixing. Iron(III) chloride aerosol generated via a 1.7 MHz ultrasonic transducer was carried by a 125 sccm (standard cubic centimeter) N₂ flow, and 3,4-ethylenedioxythiophene (EDOT) vapor generated via bubbling the liquid was carried by a 75 sccm N₂ flow. Liquid EDOT was in a 50 mL three-neck flask so that the addition of reactant was continuous. The reactor was heated to 130 $^{\circ}$ C, while the EDOT monomer temperature was 50 $^{\circ}$ C. Particles were collected as dispersion by directing aerosol flow through three ethanol-filled scrubbing bottles connected in series.

Solvent removal of collected PEDOT in ethanol dispersion was carried out in a rotary evaporator at 50 mL aliquots. The remaining dispersion was subsequently purified by centrifuging in 50% 1 M hydrochloric acid and 50% ethanol until the supernatant became colorless or light blue. Hydrochloric acid removed any iron from particles and doped the polymer. The purified dispersion was lyophilized resulting in a blue powder.

Spectroscopic Characterization. Scanning electron microscopy and energy-dispersive X-ray spectroscopy data were collected using a JEOL 7001LVF FESEM and a Thermofisher Quattro S ESEM, respectively. The samples were prepared by dispersing PEDOT particles in water and drop casting on gold-coated polyimide tape. Optical microscopy images were collected using a Nikon microscope (NIKON Eclipse, LV100ND) fitted with a Nikon Ds-Ri2 camera. Powder X-ray diffraction spectra were collected using a Bruker d8 advance X-ray diffractometer at room temperature, with a Cu Klpharadiation source ($\lambda = 1.5406 \text{ Å}$) and LynxEyeXE detector, operating at 40 kV and 40 mA. Dry sample powders were cast onto a zerointensity silicon wafer and the sample holder was rotated at 30 rpm/ min with a scan step of 0.02° . Ultraviolet-visible-near-infrared spectra were collected on a Cary 5000 ultraviolet-visible-NIR (UVvis-NIR) spectrophotometer using a parallel liquid cell. Solid powders were dispersed in 1 M HCl aqueous solutions via bath sonication and the spectra were immediately collected to minimize

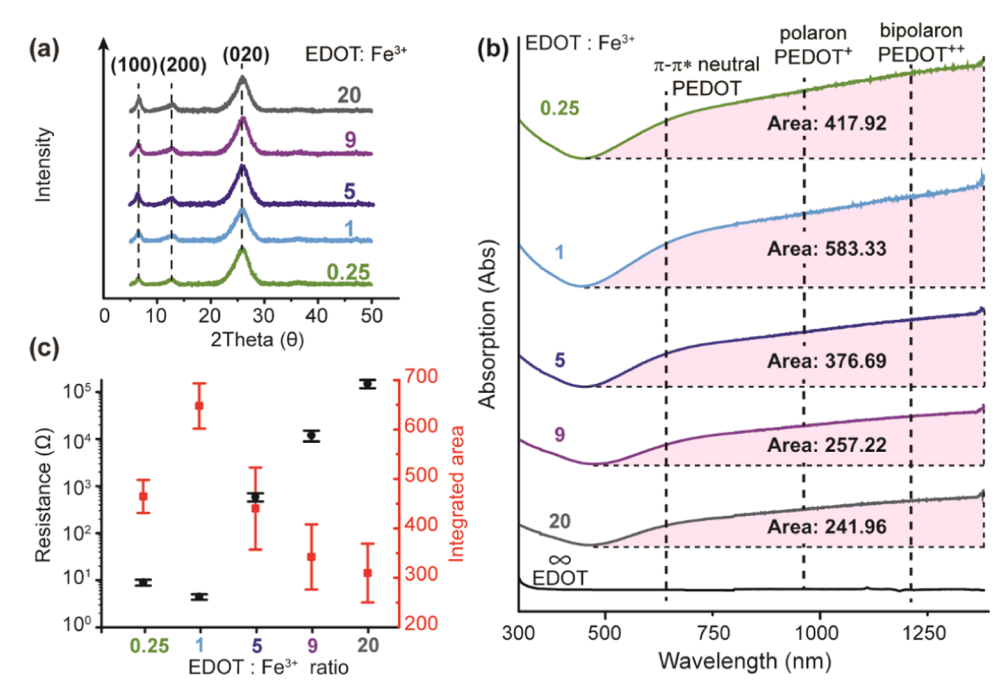


Figure 2. (a) Powder X-ray diffraction patterns for PEDOT particles synthesized under varying EDOT-to-Fe³⁺ ratios. (b) UV-vis-NIR spectra for PEDOT particles synthesized under varying EDOT-to-Fe3+ ratios and EDOT monomer. (c) Plot shows that electrical resistance is inversely proportional to the UV-vis-NIR integrated area under the curve (450-1370 nm).

the effect of particle precipitation; the data was collected in a quartz cuvette. Each measurement requires a small amount of sample (<1 mg), allowing for batch processing.

Electrochemical and Thermogravimetric Characterizations of PEDOT Particle Electrodes. The electrochemical setup consisted of a PEDOT particle working electrode, an Ag/AgCl reference electrode, a platinum mesh counter electrode, and an aqueous 1 M H₂SO₄ electrolyte. Cyclic voltammograms were collected using a BioLogic VMP3 multipotentiostat. The active mass of the working electrode was determined via thermogravimetric analysis (TGA) using a Discovery TGA (TA Instruments). The cycled electrode was rinsed thrice using water and dried in air at 25 °C before loading onto the sample pans (high-temperature Pt pans). The ramping recipe consisted of two steps: (1) 50 to 110 °C at 20 °C/min then maintained at 110 °C for 5 min to evaporate free water and (2) 110 to 500 $^{\circ}$ C at 15 $^{\circ}$ C/min then maintained at 500 $^{\circ}$ C for 30 min to burn off all the active materials (Figure S8a). The total mass loss of the second step was the total mass of PEDOT and PLA because both PEDOT and PLA were fully degraded before the temperature reached 500 °C, while the mass loss of carbon paper was negligible (Figure S8b). Air was required to fully burn off all active materials on the carbon paper; if N₂ was used, residual active materials would remain in the electrode, resulting in inaccurate mass determination (Figure

Paint Formulations and Functionalized 3D-Printed Objects.

Organic paint formulation for thermoplastics consisted of 33 wt % PEDOT particles, 67 wt % polycaprolactone, and 1 mL of trifluoroethanol (per 100 mg solids). All components were mixed using bath sonication for 1 h and brush painted onto 3D prints to form the coating. Organic paint formulation for carbon paper electrode consisted of 90 wt % PEDOT particles, 10 wt % polylactic acid, and 1 mL of chloroform. All components were thoroughly mixed using bath sonication for 1 h, and a PEDOT particle electrode was fabricated by drop casting 50 µL of the dispersion onto a piece of carbon paper (1.5 cm × 1 cm). 3D-printed objects were designed in Rhino or downloaded from the open-source website www. thinginverse.com and sliced using the software Simplify 3D. Makergear M2 was used as the FDM-based 3D printer.

An 808 nm laser was used as the NIR source, and an IR camera (ICI 7320 USB camera) was used to monitor the temperature. An

aluminum foil was placed under the samples as background due to its low infrared light absorbance.

RESULTS AND DISCUSSIONS

PEDOT Particles of High Electrical Conductivity. PEDOT particles are synthesized when a stream of aerosolized aqueous FeCl3 droplets reacts with EDOT vapor inside a flow reactor (Figure 1a). The reactor is optimized from our previous studies to achieve continuous polymerization (details in materials and methods) within 1 min of residence time. 25,26 Particles are collected in ethanol-filled scrubbing bottles, then purified, and dried, resulting in a powder (Figure 1b) comprised of spherical particles (Figures 1c and S1) readily dispersible in water (Figure 1c inset). Electrical resistance, measured by pressing particles over a 1 mm gap electrode (Figure S2), is the lowest reported among PEDOT particles (4.2 \pm 0.5 Ω). A pressed pellet enhances probe contact, facilitating I-V measurements that result in linear curves with an ohmic window ranging between -2 and 2 V. The slope increases upon exposure to HCl vapor (Figure 1d).

During synthesis, oxidative doping imparts electrical conductivity to the polymer chains by introducing mobile charge carriers (polarons, bipolarons).²⁷ According to the Drude model ($\sigma = qn\mu$),²⁸ high electrical conductivity is achieved when charge-carrier concentration (n) and mobility (μ) are maximized (q is a unit charge). To achieve high electrical conductivity, a polymer's molecular structure must possess (1) a long conjugation length to accommodate a high concentration of charge carriers (doping level)^{29,30} and (2) ordered chain packing (crystallinity) enabling high mobility of charge carriers.³¹ The oxidative radical polymerization of conducting polymers follows a step-growth mechanism 30,32 concomitant with oxidative doping after each step of chain coupling.³⁰ Therefore, synthetic conditions are of paramount importance for controlling a polymer's molecular structure and its electrical properties. Our synthesis requires (1) aerosoliza-

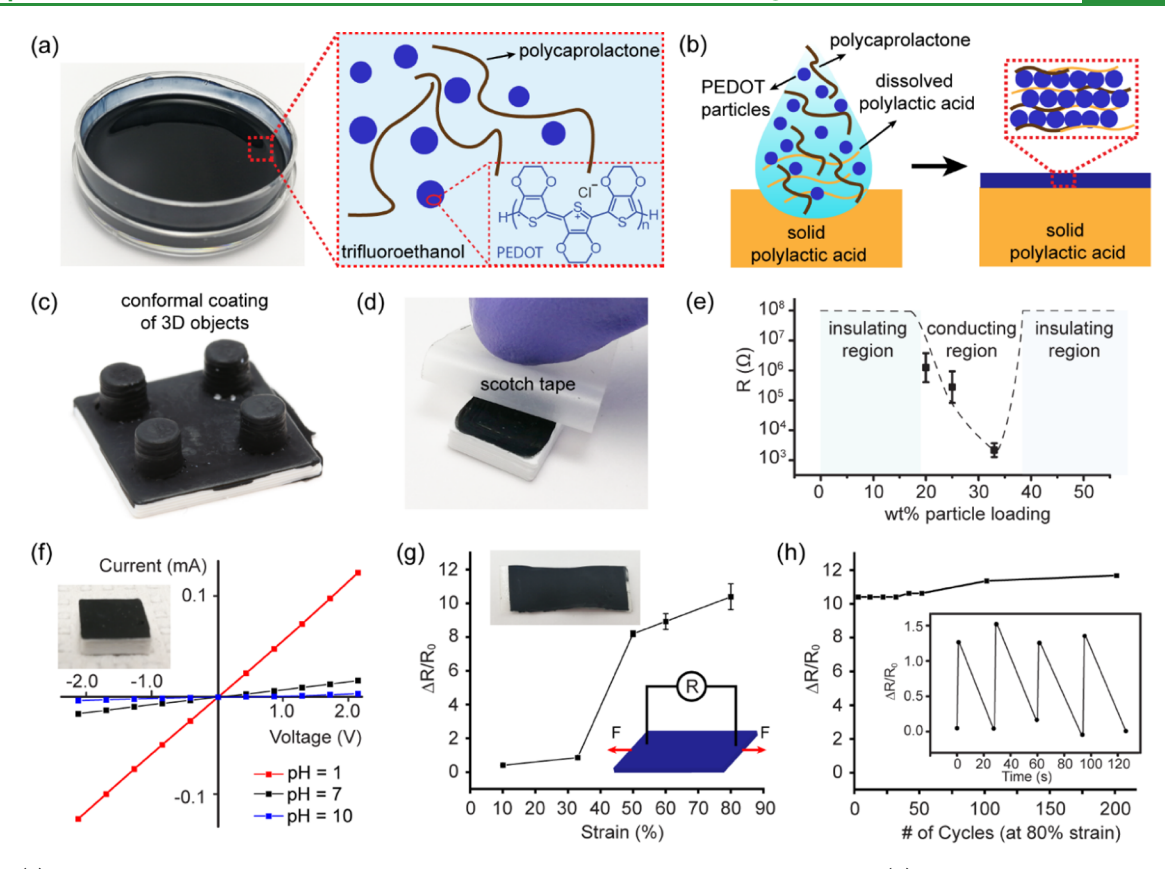


Figure 3. (a) Photograph of a PEDOT particle-based dispersion and illustration of its composition. (b) Diagram showing the dissolution of polylactic acid surface and the formation of a coating. (c) Conformal coating on a 3D-printed object is (d) impervious to delamination after repeated Scotch tape tests. (e) Plot of a coating's two-point electrical resistance versus particle mass loading. (f) Particle-coated thermoplastic polylactic acid block (inset) exhibits linear I-V curves after exposure to vapors of different pH values. (g) Resistance versus strain plot for a particle-coated thermoplastic polyurethane film (top inset) serving as a strain sensor (bottom inset). (h) Strain sensor is stable over 200 cycles (the inset shows the hysteresis profile).

tion of oxidant (FeCl₃ solution) and (2) vaporization of liquid monomer (EDOT), the former is achieved using an ultrasonic transducer and the latter by heating a nitrogen-pushed bubbler.²⁵ The product that flows out of the aerosol reactor is comprised of a mixture of PEDOT particles, unreacted liquid oxidant droplets, monomer vapor, and byproducts (reduced oxidant or EDOT oligomers).

Particles collected in the ethanol dispersion show a blue color, characteristic of doped PEDOT. The color of ethanol also changes due to excess oxidant (yellow) or excess monomer (purple) (Figure S3). The morphology of washed particles also varies as the ratio between EDOT and Fe3+ changes. The synthesized particles are perforated spheres when the reactor contains a much higher concentration of EDOT than Fe³⁺. Shriveled/walnut-shaped particles are formed when excess Fe³⁺ is present in the reactor (Figure S4). We added an additional figure to the Supporting Information File to demonstrate this in detail. The crystallinity, doping levels, and electrical resistance of PEDOT particles are studied as a function of stoichiometry by varying the EDOT-to-Fe³⁺ ratio (0.25, 1, 5, 9, 20) using samples labeled PEDOT (1:4), PEDOT (1:1), PEDOT (5:1), PEDOT (9:1), and PEDOT (20:1), respectively. Polymer crystallinity is examined via powder X-ray diffraction (XRD), a fast and nondestructive technique. 33,34 All XRD patterns exhibit three peaks (characteristic of PEDOT), 35 where the first two $(2\theta = 6.5^{\circ})$ and $2\theta = 6.5^{\circ}$ 12.8°) represent edge-on packing for the (100) and (200) planes, respectively (interplanar distance = 1.32 nm). The third

peak $(2\theta = 25.9^{\circ})$, due to face-on $\pi - \pi$ stacking of the (020) plane, exhibits a d-spacing (0.41 nm) smaller than that of a single crystalline PEDOT nanowire.³¹ This short $\pi - \pi$ distance facilitates high charge mobility,²⁸ leading to high electrical conductivity in the particles. The packing of polymer chains is independent of stoichiometry as demonstrated by a negligible difference in the number and position of XRD peaks (Figure 2a). Our PEDOT particles possess higher crystallinity than those synthesized from solution phase^{26,36,37} due to size-constrained polymerization at the micron-sized aerosol droplet's surface facilitating $\pi - \pi$ stacking.³¹

The doping level of PEDOT particles is quantitatively probed via UV-vis-NIR absorption spectroscopy. Particles are doped in a 1 M HCl solution (0.1 mg/mL) to eliminate variations in the spectra due to unleveled protonic doping.²⁵ Results show that the EDOT-to-Fe³⁺ ratio controls the area under the curve in the free charge-carrier region (450-1370 nm) (Figure 2b). This region is chosen because it maximizes the signal-to-noise ratio. The integrated area under the curve (baseline against the lowest point on a spectrum) exhibits an inverse and proportional relationship with PEDOT's electrical resistance (measured using a 1 mm gap electrode) (Figure 2c) due to polaronic and bipolaronic charge carriers. A larger area corresponds to a greater charge-carrier concentration based on the Beer-Lambert law,³⁸ resulting in lower electrical resistance. Neutral π - π * is not considered a charge carrier in PEDOT chains,²⁷ but it aids in determining the extent of conjugation because the spectrum for EDOT lacks $\pi - \pi^*$

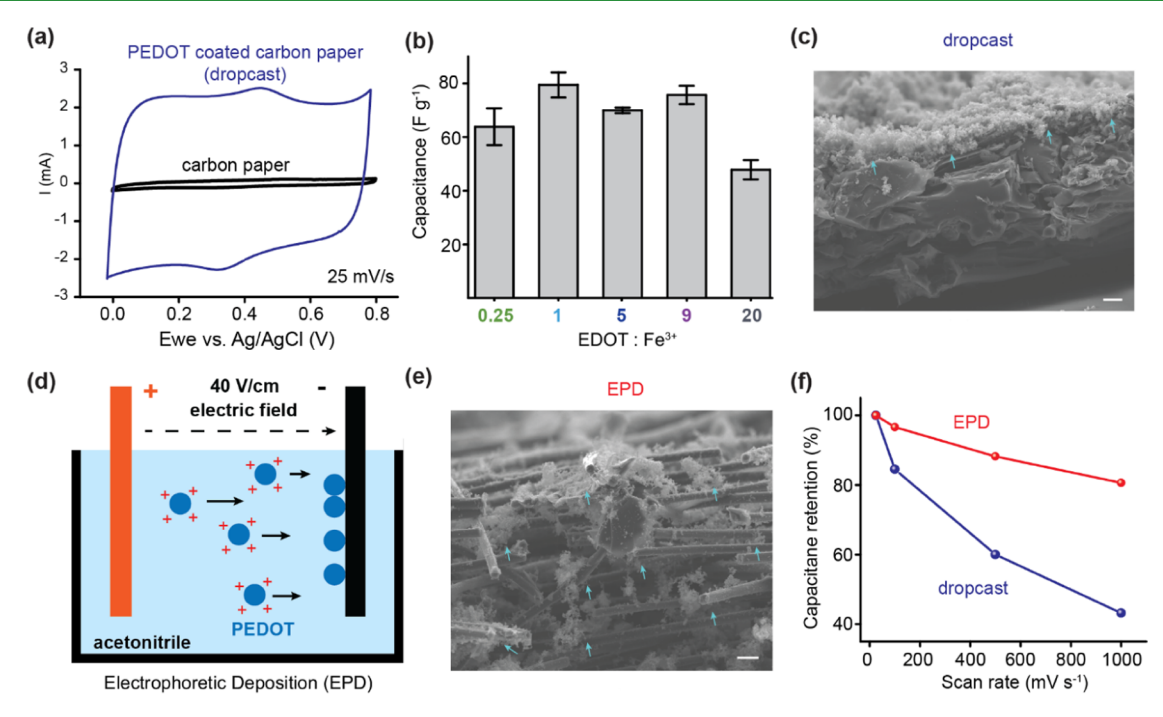


Figure 4. (a) Cyclic voltammograms of carbon paper and PEDOT particle-coated carbon paper produced via drop casting (electrode). (b) Specific capacitance plot for electrodes produced using particles synthesized from various EDOT-to-Fe³⁺ ratios (calculated from cyclic voltammograms at 25 mV/s). (c) Cross-sectional scanning electron micrograph for an electrode fabricated via drop casting (blue arrows indicate particles, scale bar = 10 μ m). (d) Illustration of electrophoretic deposition. (e) Cross-sectional scanning electron micrograph for an electrode fabricated via electrophoretic deposition shows particles integrated within carbon fibers (blue arrows indicate particles, scale bar = 10 μ m). (f) Capacitance retention plot compares electrodes fabricated via electrophoretic deposition versus drop casting.

transitions, as well as polarons and bipolarons (Figure 2b bottom curve). Therefore, a magnitude of 500 for the integrated area under the curve in the free charge-carrier region serves as an indicative test for selecting PEDOT batches of high conductivity.

PEDOT Particle-Based Coatings on Untreated Thermoplastics. To produce a homogeneous conductive coating on untreated 3D-printed thermoplastics (Figure 3a), such as polylactic acid (PLA), polyethylene terephthalate glycol (PETG), and thermoplastic polyurethane (TPU), a paint formulation comprised of PEDOT particles, trifluoroethanol (solvent) and polycaprolactone (thickener), is developed. The formulation obviates the need for a primer³⁹ because trifluoroethanol partially dissolves the thermoplastic, resulting in strong particle adhesion to a 3D-printed object. Trifluoroethanol's moderate evaporation rate (vapor pressure of 7 kPa at 20 °C)⁴⁰ facilitates the deposition of PEDOT and prevents particles from agglomerating during drying 41 (Figure 3b). Our coating is conformal (Figure 3c), and particles remain adhered after repeated scotch tape tests (Figure 3d), whereas a PEDOT:PSS produces a nonconformal coating that readily delaminates from the surface of a 3D-printed object after drying (Figure S5). At 20 wt % particle loading, a percolation network⁴² is achieved and the coating becomes conductive, while a 30 wt % particle loading (PEDOT:polycaprolactone volume ratio of 1:2) produces a 1 k Ω electrical resistance (measured via two-point technique with a 1 cm gap) (Figure 3e). Increasing the loading beyond 30 wt % induces cracks during drying and results in a partially insulating coating. Our electrical resistance is lower than that of a 3D-printed object produced from a commercial conductive 3D printing filament (1.8 k Ω). Moreover, applying our formulation obviates the issues of nozzle cracking and low printing fidelity that often

accompany 3D printing with a conductive filament laden with carbon particles. 43,44

Coating a 3D-printed object with our formulation enables the engineering of a chemically resistive pH sensor. PEDOT particles are sensitive to pH changes, acidic pH lower PEDOT's resistance due to protonic doping⁴⁵ while bases increase its resistance due to dedoping.⁴⁶ Changes in electrical resistance are measured using a two-point current–voltage technique after exposure to acid (HCl) or base (NH₄OH) vapors (Figure 3f inset); a linear correlation with the steepest slope corresponding to the lowest electrical resistance is obtained upon exposure to the HCl vapor (pH = 1) (Figure 3f).

A particle-based formulation also enables the engineering of a strain sensor when applied as a coating to an untreated 3Dprinted stretchable polyurethane substrate (Figure 3g top left inset). Electrical resistance is measured during repeated stretch-release cycles using a multimeter (Figure 3g bottom right inset). The relative resistance change $(\Delta R/R_0)$ is highly reproducible within a wide strain range (0-80%) and comparable to that of a strain sensor fabricated from silver nanowires, reduced graphene oxide, and polyurethane. 47 ΔR R_0 follows an approximately linear trend that increases with greater strain (Figure 3g). A sharp jump in slope is observed when strain increases from 33 to 50% due to the formation of cracks (Figure S6) that disrupt the conductive percolation network. The measurement is reproducible because PEDOT particles strongly adhere to polyurethane surfaces and the conductive percolation network is restored once the polyurethane returns to its original shape.⁴⁸ The strain sensor is stable for up to 200 cycles (at 80% strain) (Figure 3h). Interestingly, the coating also enables monitoring of strain

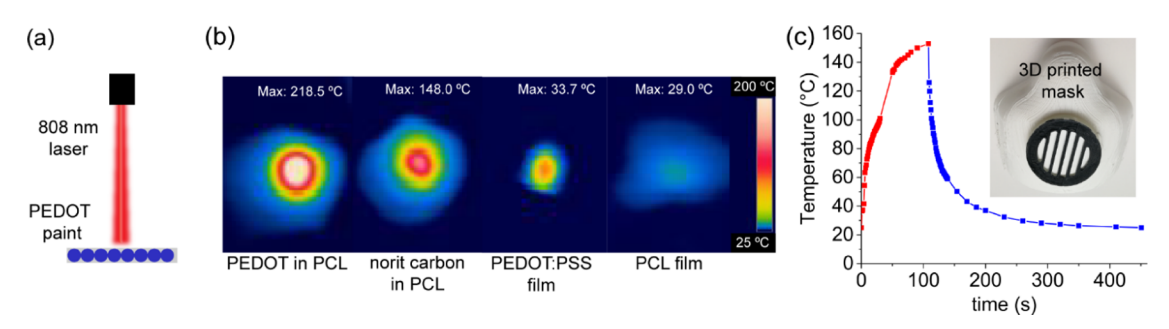


Figure 5. (a) Illustration of the photothermal experiment (808 nm laser). (b) Temperature distribution for films comprised of PEDOT–polycaprolactone, Norit carbon–polycaprolactone, PEDOT:PSS on glass, and pristine polycaprolactone after a 5 s laser exposure (power density 0.8 W/cm²). (c) Temperature profile for a PEDOT-coated 3D-printed polyethylene terephthalate glycol mask during and after laser exposure (inset shows a photograph of the mask).

sensor hysteresis, exhibiting a \sim 20 s delay when returning to its original shape after experiencing 33% strain (Figure 3h inset).

PEDOT Particle-Based Coatings on Carbon Fiber Paper. Carbon fiber paper is an ideal substrate for electrochemical applications, and our particles produce robust coatings on carbon substrates when formulated using chloroform (solvent) and polylactic acid (ion-permeable binder).⁴⁹ An electroactive and mechanically robust particle-based coating on carbon fiber paper is comprised of 10 wt % particle loading, and the working electrode is fabricated via drop casting. A three-electrode configuration is employed for measuring the gravimetric capacitance (details in materials and methods), and a quasi-rectangular cyclic voltammogram (25 mV/s) reveals the capacitive behavior of PEDOT particles^{50,51} with negligible contribution from carbon paper (Figure 4a). Redox peaks at 0.4V (vs Ag/AgCl), likely stemming from residual iron species, diminish as the scan rate increases to 1000 mV/s because faradic processes occur faster in PEDOT than in iron species.⁵¹ The PEDOT (1:1) sample possesses the highest gravimetric capacitance (80 F/g at 25 mV/s) and the lowest electrical resistance among all samples (Figure 4b) and represents the state-of-the-art among reported PEDOT particle-based electrodes. 52,53

Fabricating electrodes via drop casting presents two drawbacks: (1) particles aggregate on the carbon paper surface (Figure 4c) and (2) an insulating binder is required for immobilizing particles. Both stifling features are detrimental to charge transport between the polymer and current collector, 54 causing the cyclic voltammogram to shrink to a fusiform shape with a 55% capacitance loss when the cycling rate increases to 1000 mV/s (Figure S7a,b). Electrophoresis is a deposition technique that overcomes the challenges in drop casting by obviating the need for insulating binders. In the electrophoretic deposition, an electrical field is applied across a colloidal dispersion, allowing positively charged particles to migrate to the negative substrate. As a result, a stable coating is formed and able to undergo repeated electrochemical cycling.⁵⁴ Electrophoretic deposition at 40 V/cm is utilized to deposit positively charged particles to fabricate a working electrode, and a porous carbon paper serves as a current collector (PEDOT (1:1) sample, dispersed in acetonitrile, 1 mg/mL) (Figure 4d). A homogeneous particle coating is deposited throughout the porous carbon current collector (Figure 4e), facilitating facile charge transport at the interface. Moreover, small capacitance loss (<20%) (Figure 4f), with a quasirectangular cyclic voltammogram (collected from 25 to 1000 mV/s) (Figure S7c), indicates a high-performance electrode.

Particle Coatings with High Photothermal Activity. A

PEDOT particle-based coating is photothermally active in the near-infrared region. After a 5 s laser exposure (808 nm laser, 0.8 W/cm² power density) (Figure 5a), a freestanding PEDOT particle—polycaprolactone composite film (24 °C) heats up to 218.5 °C. This temperature increase (194.5 °C) is higher than that of a Norit carbon/polycaprolactone composite film (124 °C) or a PEDOT:PSS film (9.7 °C). PEDOT particles are the major contributors to the temperature increase, and a pure polycaprolactone film shows a <5 °C increase after the same exposure (Figure 5b). Our coating's temperature increase is also higher than those of other reported PEDOT films²3,24 because particle boundaries lower the heat dissipation rate, creating a heat confinement effect. The light from a camera flash ignites a cotton ball impregnated with PEDOT particles (Supporting Movie).

The spread of COVID-19 since 2020 affects human life profoundly and masks are an effective prevention against the spreading of the virus. Unfortunately, the increased use of disposable masks also generates a large amount of plastic waste and is forcing us to look for alternatives. 3D printing is a promising technique for fast prototyping reusable masks. However, masks are reusable only if the surface is effectively disinfected after each use. Utilizing the photothermal property of PEDOT coatings as a fast, nondestructive microbial ablation method, a proof-of-concept reusable mask is proposed. 56 Brushing the PEDOT particle-based formulation on the air filter cap of a 3D-printed polyethylene terephthalate glycol mask (Figure 5c inset) and exposing it to a laser for 100 s (808 nm, 0.8 W/cm²) increase the surface temperature to 150 °C, a temperature that is sufficient for inactivating COVID-19.5 The temperature increase is lower than that of a freestanding PEDOT particle-polycaprolactone composite film because the 3D-printed polyethylene terephthalate glycol mask absorbs heat. The surface temperature drops after the laser is turned off (Figure 5c), and the mask structure and particle coating remain intact.

CONCLUSIONS

We develop a continuous synthesis of PEDOT particles with an optimized low resistance of 4.2 \pm 0.5 Ω measured by a 1 mm gap electrode. Tuning the EDOT-to-Fe $^{3+}$ ratio reveals that stoichiometry affects PEDOT's crystallinity, doping level, and electrical and electrochemical properties. Results show that a balanced EDOT-to-Fe $^{3+}$ ratio (1:1) leads to the highest charge-carrier concentration responsible for the lowest electrical resistance among samples. A highly stable electrode

is fabricated via electrophoretic deposition of PEDOT particles on carbon fiber paper. The electrode is characterized by cyclic voltammetry and possesses a state-of-the-art gravimetric capacitance for PEDOT particles. Particles are readily processable as a colloidal dispersion and we formulate an organic paint that conformally coats 3D-printed thermoplastic objects, resulting in a low electrical resistance (1 k Ω /cm), comparable to prints produced from commercial conductive filaments. A particle coating enables the fabrication of 3D-printed pH sensors, strain sensors, and affords a light-induced method for triggering rapid heating of a PEDOT-coated surface.

ASSOCIATED CONTENT

5 Supporting Information

The Supporting Information is available free of charge at https://pubs.acs.org/doi/10.1021/acsami.2c18328.

Flash ignition of a PEDOT particle-impregnated cotton ball (MP4)

Solution-processable PEDOT particles for coatings of untreated 3D-printed Thermoplastics (PDF)

AUTHOR INFORMATION

Corresponding Author

Julio M. D'Arcy — Institute of Materials Science & Engineering, Washington University in St. Louis, St. Louis, Missouri 63130, United States; Department of Chemistry, Washington University in St. Louis, St. Louis, Missouri 63130, United States; Present Address: Department of Chemistry and Biochemistry, Clark University, Worcester, Massachusetts 01610, United States; orcid.org/0000-0002-6823-3586; Email: judarcy@clarku.edu

Authors

Yang Lu — Institute of Materials Science & Engineering, Washington University in St. Louis, St. Louis, Missouri 63130, United States; Present Address: School of Engineering and Applied Sciences, Harvard University, Boston, Massachusetts 02134, United States

Haoru Yang — Department of Chemistry, Washington University in St. Louis, St. Louis, Missouri 63130, United States; Occid.org/0000-0001-6761-5868

Yifan Diao — Institute of Materials Science & Engineering, Washington University in St. Louis, St. Louis, Missouri 63130, United States; Present Address: Central R&D Institute, LONGi Green Energy Technology Co. Ltd., Shanghai 200120, China

Hongmin Wang — Department of Chemistry, Washington University in St. Louis, St. Louis, Missouri 63130, United States; Present Address: Department of Chemistry, Yale University, New Haven, Connecticut 06520, United States; Energy Sciences Institute, Yale University, West Haven, Connecticut 06516, United States; orcid.org/0000-0003-2714-4250

Chiemela Izima — Department of Chemistry, Washington University in St. Louis, St. Louis, Missouri 63130, United States; Present Address: Vagelos College of Physicians and Surgeons, Columbia University, New York 10032, United States

Imani Jones – Department of Chemistry, Washington University in St. Louis, St. Louis, Missouri 63130, United States Reagan Woon — Department of Chemistry, Washington University in St. Louis, St. Louis, Missouri 63130, United States; Present Address: Spinger Nature, London N1 9XW, United Kindom

Kenneth Chrulski – Department of Chemistry, Washington University in St. Louis, St. Louis, Missouri 63130, United States

Complete contact information is available at: https://pubs.acs.org/10.1021/acsami.2c18328

Author Contributions

◆Y.L. and H.Y. contributed equally to this work. The manuscript was written through contributions of all authors. All authors have given approval to the final version of the manuscript.

Funding

Leadership and Entrepreneurial Acceleration Program from the Skandalaris Center for Interdisciplinary Innovation and Entrepreneurship at Washington University in St. Louis. Start-up fund from the chemistry department at Clark University.

Notes

The authors declare no competing financial interest.

ACKNOWLEDGMENTS

The authors greatly acknowledge the help from Prof. Young-Shin Jun and Dr. Deoukchen Ghim on the photothermal instrumentations. They thank Prof. Srikanth Singamaneni and Dr. Prashant Gupta for their help with the 808 nm laser and IR temperature monitor. Y.L. thanks Prof. Bryce Sadtler for use of their instruments and Dr. Meikun Shen for fruitful discussions. Y.L thanks Prof. Richard Loomis for use of their instruments and Dr. Jie Chen for help on the instrumentations.

REFERENCES

- (1) Billah, K. M. M.; Coronel, J. L.; Halbig, M. C.; Wicker, R. B.; Espalin, D. Electrical and Thermal Characterization of 3D Printed Thermoplastic Parts with Embedded Wires for High Current-Carrying Applications. *IEEE Access* **2019**, *7*, 18799–18810.
- (2) Alafaghani, A.; Qattawi, A.; Ablat, M. A. Design Consideration for Additive Manufacturing: Fused Deposition Modelling. *Open J. Appl. Sci.* **2017**, *07*, 291–318.
- (3) Liaw, C. Y.; Guvendiren, M. Current and Emerging Applications of 3D Printing in Medicine. *Biofabrication* **2017**, *9*, No. 024102.
- (4) Gulzar, U.; Glynn, C.; O'Dwyer, C. Additive Manufacturing for Energy Storage: Methods, Designs and Material Selection for Customizable 3D Printed Batteries and Supercapacitors. *Curr. Opin. Electrochem.* **2020**, 20, 46–53.
- (5) Griffey, J. 3-D Printers for Libraries; American Library Association, 2014; Vol. 50.
- (6) Flowers, P. F.; Reyes, C.; Ye, S.; Kim, M. J.; Wiley, B. J. 3D Printing Electronic Components and Circuits with Conductive Thermoplastic Filament. *Addit. Manuf.* **2017**, *18*, 156–163.
- (7) Someya, T.; Bao, Z.; Malliaras, G. G. The Rise of Plastic Bioelectronics. *Nature* **2016**, *540*, *379*–*385*.
- (8) Rivnay, J.; Inal, S.; Salleo, A.; Owens, R. M.; Berggren, M.; Malliaras, G. G. Organic Electrochemical Transistors. *Nat. Rev. Mater.* **2018**, 3, No. 17086.
- (9) Bubnova, O.; Khan, Z. U.; Malti, A.; Braun, S.; Fahlman, M.; Berggren, M.; Crispin, X. Optimization of the Thermoelectric Figure of Merit in the Conducting Polymer Poly(3,4-Ethylenedioxythiophene). *Nat. Mater.* **2011**, *10*, 429–433.
- (10) Berggren, M.; Malliaras, G. G. How Conducting Polymer Electrodes Operate. *Science* **2019**, *364*, 233–234.

- (11) Guo, X.; Facchetti, A. The Journey of Conducting Polymers from Discovery to Application. *Nat. Mater.* **2020**, *19*, 922–928.
- (12) Mitraka, E.; Gryszel, M.; Vagin, M.; Jafari, M. J.; Singh, A.; Warczak, M.; Mitrakas, M.; Berggren, M.; Ederth, T.; Zozoulenko, I.; Crispin, X.; Głowacki, E. D. Electrocatalytic Production of Hydrogen Peroxide with Poly(3,4-Ethylenedioxythiophene) Electrodes. *Adv. Sustainable Syst.* **2019**, *3*, No. 1800110.
- (13) Ghosh, S.; Kouame, N. A.; Remita, S.; Ramos, L.; Goubard, F.; Aubert, P. H.; Dazzi, A.; Deniset-Besseau, A.; Remita, H. Visible-Light Active Conducting Polymer Nanostructures with Superior Photocatalytic Activity. *Sci. Rep.* **2015**, *5*, No. 18002.
- (14) Valiollahi, R.; Vagin, M.; Gueskine, V.; Singh, A.; Grigoriev, S. A.; Pushkarev, A. S.; Pushkareva, Iv.; Fahlman, M.; Liu, X.; Khan, Z.; Berggren, M.; Zozoulenko, I.; Crispin, X. Electrochemical Hydrogen Production on a Metal-Free Polymer. *Sustainable Energy Fuels* **2019**, 3, 3387–3398.
- (15) Horii, T.; Li, Y.; Mori, Y.; Okuzaki, H. Correlation between the Hierarchical Structure and Electrical Conductivity of PEDOT/PSS. *Polym. J.* **2015**, *47*, 695–699.
- (16) Seekaew, Y.; Lokavee, S.; Phokharatkul, D.; Wisitsoraat, A.; Kerdcharoen, T.; Wongchoosuk, C. Low-Cost and Flexible Printed Graphene-PEDOT:PSS Gas Sensor for Ammonia Detection. *Org. Electron.* **2014**, *15*, 2971–2981.
- (17) Yuk, H.; Lu, B.; Lin, S.; Qu, K.; Xu, J.; Luo, J.; Zhao, X. 3D Printing of Conducting Polymers. *Nat. Commun.* **2020**, *11*, No. 1604.
- (18) Jordan, R. S.; Wang, Y. 3D Printing of Conjugated Polymers. J. Polym. Sci., Part B: Polym. Phys. 2019, 57, 1592–1605.
- (19) Xia, Y.; Ouyang, J. PEDOT:PSS Films with Significantly Enhanced Conductivities Induced by Preferential Solvation with Cosolvents and Their Application in Polymer Photovoltaic Cells. *J. Mater. Chem.* **2011**, 21, 4927–4936.
- (20) Lei, Y.; Oohata, H.; Kuroda, S. I.; Sasaki, S.; Yamamoto, T. Highly Electrically Conductive Poly(3,4-Ethylenedioxythiophene) Prepared via High-Concentration Emulsion Polymerization. *Synth. Met.* **2005**, *149*, 211–217.
- (21) Pang, R.; Hu, X.; Zhou, S.; Sun, C.; Yan, J.; Sun, X.; Xiao, S.; Chen, P. Preparation of Multi-Shelled Conductive Polymer Hollow Microspheres by Using Fe3O4 Hollow Spheres as Sacrificial Templates. *Chem. Commun.* **2014**, *50*, 12493–12496.
- (22) Zhang, X.; MacDiarmid, A. G.; Manohar, S. K. Chemical Synthesis of PEDOT Nanofibers. *Chem. Commun.* **2005**, 42, 5328–5330.
- (23) Kim, B.; Han, M.; Kim, E. Photothermally Powered Conductive Films for Absorber-Free Solar Thermoelectric Harvesting. *J. Mater. Chem. A* **2019**, 7, 2066–2074.
- (24) Lim, H.; Park, T.; Na, J.; Park, C.; Kim, B.; Kim, E. Construction of a Photothermal Venus Flytrap from Conductive Polymer Bimorphs. *NPG Asia Mater.* **2017**, *9*, No. e399.
- (25) Lu, Y.; Kacica, C.; Bansal, S.; Santino, L. M.; Acharya, S.; Hu, J.; Izima, C.; Chrulski, K.; Diao, Y.; Wang, H.; Yang, H.; Biswas, P.; Schaefer, J.; D'Arcy, J. M. Synthesis of Submicron PEDOT Particles of High Electrical Conductivity via Continuous Aerosol Vapor Polymerization. ACS Appl. Mater. Interfaces 2019, 11, 47320–47329.
- (26) Zhang, Y.; Suslick, K. S. Synthesis of Poly(3,4-Ethylenedioxythiophene) Microspheres by Ultrasonic Spray Polymerization (USPo). *Chem. Mater.* **2015**, *27*, 7559–7563.
- (27) Zozoulenko, I.; Singh, A.; Singh, S. K.; Gueskine, V.; Crispin, X.; Berggren, M. Polarons, Bipolarons, and Absorption Spectroscopy of PEDOT. ACS Appl. Polym. Mater. 2019, 1, 83–94.
- (28) Gharahcheshmeh, M. H.; Tavakoli, M. M.; Gleason, E. F.; Robinson, M. T.; Kong, J.; Gleason, K. K. Tuning, Optimization, and Perovskite Solar Cell Device Integration of Ultrathin Poly(3,4-Ethylene Dioxythiophene) Films via a Single-Step All-Dry Process. *Sci. Adv.* 2019, 5, No. eaay0414.
- (29) Lock, J. P.; Im, S. G.; Gleason, K. K. Oxidative Chemical Vapor Deposition of Electrically Conducting Poly(3,4-Ethylenedioxythiophene) Films. *Macromolecules* **2006**, *39*, 5326–5329.

- (30) Kim, D.; Zozoulenko, I. Why Is Pristine PEDOT Oxidized to 33%? A Density Functional Theory Study of Oxidative Polymerization Mechanism. *J. Phys. Chem. B* **2019**, *123*, 5160–5167.
- (31) Cho, B.; Park, K. S.; Baek, J.; Oh, H. S.; Koo Lee, Y. E.; Sung, M. M. Single-Crystal Poly(3,4-Ethylenedioxythiophene) Nanowires with Ultrahigh Conductivity. *Nano Lett.* **2014**, *14*, 3321–3327.
- (32) Aplan, M. P.; Gomez, E. D. Recent Developments in Chain-Growth Polymerizations of Conjugated Polymers. *Ind. Eng. Chem. Res.* **2017**, *56*, 7888–7901.
- (33) Patel, A. K.; Bajpai, R.; Keller, J. M. On the Crystallinity of PVA/Palm Leaf Biocomposite Using DSC and XRD Techniques. *Microsyst. Technol.* **2014**, 20, 41–49.
- (34) Sami, A.; David, E.; Fréchette, M. Procedure for Evaluating the Crystallinity from X-Ray Diffraction Scans of High and Low Density Polyethylene/SiO2 Composites, 2010 Annual Report Conference on Electrical Insulation and Dielectic Phenomena; IEEE: West Lafayette, IN. USA. 2010.
- (35) Wang, H.; Santino, L. M.; Rubin, M.; Diao, Y.; Lu, Y.; D'Arcy, J. M. Self-Woven Nanofibrillar PEDOT Mats for Impact-Resistant Supercapacitors. *Sustainable Energy Fuels* **2019**, *3*, 1154–1162.
- (36) Paradee, N.; Sirivat, A. Synthesis of Poly(3,4-Ethylenedioxythiophene) Nanoparticles via Chemical Oxidation Polymerization. *Polym. Int.* **2014**, *63*, 106–113.
- (37) Zheng, H.; Jiang, Y.; Xu, J.; Yang, Y. The Characteristic Properties of PEDOT Nano-Particle Based on Reversed Micelle Method. Sci. China Technol. Sci. 2010, 53, 2355–2362.
- (38) Lee, H.; Kim, Y.; Cho, H.; Lee, J. G.; Kim, J. H. Improvement of PEDOT:PSS Linearity: Via Controlled Addition Process. *RSC Adv.* **2019**. *9*. 17318–17324.
- (39) Mamatha, S.; Biswas, P.; Das, D.; Johnson, R. Fabrication of Complex Shaped Ceramic Articles from 3D Printed Polylactic Acid Templates by Replication Process. *Ceram. Int.* **2019**, *45*, 19577–19580.
- (40) Chaudhari, S. K.; Patil, K. R.; Allepús, J.; Coronas, A. Measurement of the Vapor Pressure of 2,2,2-Trifluoroethanol and Tetraethylene Glycol Dimethyl Ether by Static Method. *Fluid Phase Equilib.* 1995, 108, 159–165.
- (41) Munekata, T.; Suzuki, T.; Yamakawa, S.; Asahi, R. Effects of Viscosity, Surface Tension, and Evaporation Rate of Solvent on Dry Colloidal Structures: A Lattice Boltzmann Study. *Phys. Rev. E* **2013**, 88, No. 052314.
- (42) Chen, J.; Yu, Q.; Cui, X.; Dong, M.; Zhang, J.; Wang, C.; Fan, J.; Zhu, Y.; Guo, Z. An Overview of Stretchable Strain Sensors from Conductive Polymer Nanocomposites. *J. Mater. Chem. C* **2019**, *7*, 11710–11730.
- (43) Olsson, A.; Hellsing, M. S.; Rennie, A. R. New Possibilities Using Additive Manufacturing with Materials That Are Difficult to Process and with Complex Structures. *Phys. Scr.* **2017**, *92*, No. 053002.
- (44) Gnanasekaran, K.; Heijmans, T.; van Bennekom, S.; Woldhuis, H.; Wijnia, S.; de With, G.; Friedrich, H. 3D Printing of CNT- and Graphene-Based Conductive Polymer Nanocomposites by Fused Deposition Modeling. *Appl. Mater. Today* **2017**, *9*, 21–28.
- (45) He, S.; Mukaida, M.; Kirihara, K.; Lyu, L.; Wei, Q. Reversible Protonic Doping in Poly(3,4-Ethylenedioxythiophene). *Polymers* **2018**, *10*, No. 1065.
- (46) Sethumadhavan, V.; Zuber, K.; Bassell, C.; Teasdale, P. R.; Evans, D. Hydrolysis of Doped Conducting Polymers. *Commun. Chem.* **2020**, *3*, No. 153.
- (47) Li, Y.; Wang, S.; Xiao, Z. C.; Yang, Y.; Deng, B. W.; Yin, B.; Ke, K.; Yang, M. B. Flexible TPU Strain Sensors with Tunable Sensitivity and Stretchability by Coupling AgNWs with RGO. *J. Mater. Chem. C* **2020**, *8*, 4040–4048.
- (48) Tolvanen, J.; Hannu, J.; Jantunen, H. Stretchable and Washable Strain Sensor Based on Cracking Structure for Human Motion Monitoring. Sci. Rep. 2018, 8, No. 13241.
- (49) Santino, L. M.; Lu, Y.; Acharya, S.; Bloom, L.; Cotton, D.; Wayne, A.; D'Arcy, J. M. Enhancing Cycling Stability of Aqueous

Polyaniline Electrochemical Capacitors. ACS Appl. Mater. Interfaces 2016, 8, 29452-29460.

- (50) Diao, Y.; Chen, H.; Lu, Y.; Santino, L. M.; Wang, H.; D'Arcy, J. M. Converting Rust to PEDOT Nanofibers for Supercapacitors. ACS Appl. Energy Mater. 2019, 2, 3435-3444.
- (51) Wang, H.; Diao, Y.; Lu, Y.; Yang, H.; Zhou, Q.; Chrulski, K.; D'Arcy, J. M. Energy Storing Bricks for Stationary PEDOT Supercapacitors. Nat. Commun. 2020, 11, No. 3882.
- (52) Kelly, T. L.; Yano, K.; Wolf, M. O. Supercapacitive Properties of PEDOT and Carbon Colloidal Microspheres. ACS Appl. Mater. Interfaces 2009, 1, 2536-2543.
- (53) Liu, Y.; Turner, A. P. F.; Zhao, M.; Mak, W. C. Facile Synthesis of Highly Processable and Water Dispersible Polypyrrole and Poly(3,4-Ethylenedioxythiophene) Microspheres for Enhanced Supercapacitive Performance. Eur. Polym. J. 2018, 99, 332-339.
- (54) Li, G.; Martinez, C.; Semancik, S. Controlled Electrophoretic Patterning of Polyaniline from a Colloidal Suspension. J. Am. Chem. Soc. 2005, 127, 4903-4909.
- (55) Ajayan, P. M.; Terrones, M.; de la Guardia, A.; Huc, V.; Grobert, N.; Wei, B. Q.; Lezec, H.; Ramanath, G.; Ebbesen, T. W. Nanotubes in a Flash - Ignition and Reconstruction. Science 2002, 296, No. 705.
- (56) Huang, L.; Xu, S.; Wang, Z.; Xue, K.; Su, J.; Song, Y.; Chen, S.; Zhu, C.; Tang, B. Z.; Ye, R. Self-Reporting and Photothermally Enhanced Rapid Bacterial Killing on a Laser-Induced Graphene Mask. ACS Nano 2020, 14, 12045-12053.
- (57) Pastorino, B.; Touret, F.; Gilles, M.; Luciani, L.; de Lamballerie, X.; Charrel, R. N. Evaluation of Chemical Protocols for Inactivating SARS-CoV-2 Infectious Samples. Viruses 2020, 12, No. 624.

□ Recommended by ACS

UV-Blocking and Transparent Polydimethylsiloxane Film for **Improving Stability of Perovskite Photovoltaics**

Hanbin Lee, Hyo Jung Kim, et al.

MARCH 14 2023

ACS APPLIED OPTICAL MATERIALS

READ 2

Ultralow Temperature Glass Frit Encapsulation for Stable Dye-Sensitized Solar Cells

Jorge Martins, Adélio Mendes, et al.

NOVEMBER 07, 2022

ACS APPLIED ENERGY MATERIALS

READ **C**

Screen Printed Reflective Electrochromic Displays for Paper and Other Opaque Substrates

Kathrin Freitag, Peter Andersson Ersman, et al.

JANUARY 26, 2023

ACS APPLIED OPTICAL MATERIALS

READ **C**

Investigation of Reactive Silver Ink Formula for Reduced Silver Consumption in Silicon Heterojunction Metallization

Steven J. DiGregorio, Owen J. Hildreth, et al.

FEBRUARY 24, 2023

ACS APPLIED ENERGY MATERIALS

READ 2

Get More Suggestions >